Effects of diluents on the ignition of premixed H$_2$/air mixtures

Weikuo Zhang [a], Zheng Chen [a,*], Wenjun Kong [b]

[a] SKLTCS, Department of Mechanics and Aerospace Engineering, College of Engineering, Peking University, Beijing 100871, China
[b] Institute of Engineering Thermophysics, Chinese Academy of Sciences, Beijing 100190, China

ARTICLE INFO

ABSTRACT

A computational study is performed to investigate the effects of diluents on the ignition of premixed H$_2$/air mixtures. The ignition processes for fuel lean, stoichiometric, and fuel rich H$_2$/air mixed with different diluents (He, Ar, N$_2$, and CO$_2$) are simulated with detailed chemistry and variable thermodynamic and transport properties. The minimum ignition energies (MIE) for different diluents at different dilution ratios are obtained. It is found that the change of the MIE with the dilution ratio consists of two regimes: in the first regime with a small value of dilution ratio, diluent addition has little effect on the MIE and in the second regime with dilution ratio above a certain value, the MIE increases exponentially with the dilution ratio. The kinetic and radiation effects of dilution are assessed by conducting sensitivity analysis and using the optically thin model, respectively. The thermal and flame-dynamic effects of dilution, characterized by the adiabatic flame temperature and Markstein length, respectively, are also discussed. Moreover, the dilution limits for H$_2$/air mixtures at different equivalence ratios are obtained. The dilution limits predicted by present ignition calculation are found to agree well with those based on laminar flame speed measurements at micro-gravity conditions. The ranking in terms of the effectiveness on ignition inhibition for stoichiometric H$_2$/air is shown to be in the order of Ar, N$_2$, He, and CO$_2$. The dilution limit is of practical interest since it is a measure of the efficiency of the diluent in fire prevention and suppression.

1. Introduction

The inert gases such as helium, argon, nitrogen, and carbon dioxide are benign to people and the environment and can be mass produced. Therefore, they are considered to be an important class of fire extinguishers, especially for fire prevention and suppression in confined environments such as spacecraft [1–4]. In the literature, there are many studies on flame extinction caused by these diluents [5–11]. For examples, Tsjuji and Yamaoka [5] studied the influence of different diluents on the extinction fuel concentration using counter flow diffusion flames; Satio et al. [6] compared the efficiency of different diluents for the flame-extinguishing concentration; Liao et al. [7] assessed the effects of inert dilution on the flammability limits of combustible gases and vapors using a tubular flame method; Park and coworkers [8,9] studied the extinction of counter flow flames caused by different diluents; and Tang et al. [10,11] investigated the extinction of spherical diffusion flame caused by dilution.

However, besides flame extinction, ignition and flame propagation also happen in the fire extinguishing process. Therefore,

studies on the ignition and flame propagation with dilution are also important for understanding and improving fire prevention and suppression. For flame propagation, there are many studies investigating the effects of diluents on the flame propagation speed. For examples, Liu et al. [12] studied the thermal and kinetic effects of CO$_2$ dilution on the laminar flame speed of premixed H$_2$/air and CH$_4$/air; Qiao et al. [2–4] measured the laminar flame speed of H$_2$/air mixed with different diluents; Chen et al. [13] studied the effects of radiation emission and re-absorption on the propagation of premixed CH$_4$/air/CO$_2$ flames; Halter et al. [14] investigated the effects of diluents on the propagation speeds of methane and iso-octane air flames; and Hu et al. [15] measured the laminar flame speed of H$_2$/air diluted by N$_2$ and CO$_2$. However, there are only a few studies in the literature focused on the dilution effects on the ignition process. Lewis and von Elbe [16] measured the minimum ignition energy (MIE) of different fuel/oxygen/diluent mixtures and they found that different diluents have different influences on the magnitude of the MIE. Unfortunately, they did not thoroughly explain why the ignition is affected differently by different diluents. Therefore, the mechanisms of ignition with dilution are not well known and deserve further study.

Based on the motivation discussed above, numerical simulations of the ignition process are conducted in the present study for different H$_2$/air/diluent (He, Ar, N$_2$, and CO$_2$) mixtures. The

objectives of this study are twofold. First, we study the effects of different diluents on the MIE of premixed H_2/air mixtures. The change of the MIE with the dilution ratio is presented and the kinetic effect, radiation effect, thermal effect, and flame-dynamic effect of dilution are studied. Second, we determine the dilution limits for H_2/air with different equivalence ratios and diluents. The dilution limit for each diluent is of interest because it is a measure of the efficiency of the diluent in preventing or suppressing a fire.

2. Numerical method and specifications

A space-adaptive numerical solver for *Adaptive Simulation of Unsteady Reactive Flow*, A-SURF (1D), is used to simulate spherical flame initiation and propagation of different H_2/air/diluent mixtures. A-SURF has been validated and used in a series of studies on spherical flame initiation and propagation [17–23]. The details on the governing equations, numerical schemes, and code validation of A-SURF can be found in Refs. [17,21] and thus are only briefly described below.

The one-dimensional, unsteady, compressible Navier–Stokes equations for multi-component reactive flow are solved in A-SURF. The finite volume method is used to discretize the conservation governing equations in the spherical coordinate [17,21]. The second-order-accurate Strang splitting fractional-step procedure [24] is employed to separate the time evolution of the stiff reaction term from that of the convection and diffusion terms. In the first fractional step, the non-reactive flow is solved. The Runge–Kutta, central difference, and MUSCL-Hancock schemes, all of second-order accuracy, are employed for the calculation of the temporal integration, diffusive flux, and convective flux, respectively. The chemistry is solved in the second fractional step by using the VODE solver [25]. Detailed chemistry is considered and the reaction rates as well as thermodynamic and transport properties are evaluated using the CHEMKIN and TRANSPORT packages [26,27] interfaced with A-SURF. The mixture-averaged formula [26] is employed to calculate the diffusion velocity, in which the thermal diffusion of H, H_2, and He is considered. Moreover, a correction velocity is included to ensure the mass conservation [17,26]. In order to maintain adequate numerical resolution of the moving flame front, a multi-level, dynamically adaptive mesh refinement algorithm [28] is employed in A-SURF. Nine grid levels are utilized in this study and the moving reaction zone is always fully covered by the finest meshes of 8 μm in width. Grid convergence is tested to ensure the numerical accuracy.

In all simulations, the computational domain is $0 \leqslant r \leqslant 50$ cm. Zero flow velocity and zero gradients of temperature and mass fractions are enforced at both inner ($r = 0$) and outer ($r = 50$ cm) boundaries. At the initial state, the homogeneous mixture is quiescent at 298 K and atmospheric pressure. Flame initiation is achieved by spatial dependent energy deposition for a given ignition time

$$q_{ig}(r,t) = \begin{cases} \frac{E_{ig}}{\pi^{1.5} r_{ig}^3 \tau_{ig}} \exp\left[-\left(\frac{r}{r_{ig}}\right)^2\right] & \text{if } t < \tau_{ig} \\ 0 & \text{if } t \geqslant \tau_{ig} \end{cases} \quad (1)$$

where E_{ig} is the total ignition energy, τ_{ig}, the duration of the energy source, and r_{ig}, the ignition kernel radius. It is noted that the duration of the source energy and the ignition kernel size both affect the minimum ignition energy (MIE) [29,30]. Since the emphasis of this study is focused on the change of the MIE with the dilution and the dilution limit, the ignition kernel size and time are both kept constant with $\tau_{ig} = 200$ μs and $r_{ig} = 200$ μm, respectively. Frendi and Sibulkin [29] studied the dependence of the MIE on the ignition kernel size and time and it was found that the MIE becomes the lowest

and/or nearly constant for $\tau_{ig} \sim 100$ μs and $r_{ig} \sim 100$ μm. Large values of τ_{ig} and r_{ig} are used in this study so that in the simulation the temperature at the center is not too high after ignition energy deposition. Nevertheless, as will be mentioned in Section 3.2, the main results of this study are found to be independent of the ignition kernel sizes and times.

In the one-dimensional simulations, the thermal-diffusive and hydrodynamic instabilities in flame propagation cannot be captured. As observed in spherical flame experiments [4,31,32], thermal-diffusive and hydrodynamic instabilities occur only when the flame radius is above a critical value (which is usually more than 1 cm for H_2/air at atmospheric pressure) and the flame kernel is stable since it has a large positive stretch rate which stabilizes the flame propagation. Therefore, the effect of thermal-diffusive and hydrodynamic instabilities on the ignition process is negligible.

The composition of the initial fresh mixture is specified according to the molar ratio given by

$$(1-a)\frac{2\varphi H_2 + O_2 + 3.76 N_2}{2\varphi + 4.76} + aD \quad (2)$$

where φ is the equivalence ratio ($\varphi = 0.5$, 1.0, and 2.0 for fuel lean, stoichiometric, and fuel rich, respectively), D denotes the chemical formula of the diluent (He, Ar, N_2, or CO_2), and a is the dilution ratio equaling to the molar fraction of the diluent added to the mixture.

3. Results and discussions

There are many kinetic mechanisms for hydrogen oxidation with/without CO and CO_2 chemistry in the literature [33–38]. According to the comparison conducted in Section 3.3 (see Fig. 5), weak dependence of the main results on different kinetic mechanisms is observed. Therefore, except those in Fig. 5, all other results reported in this study are obtained from simulations using the kinetic mechanism developed by Li et al. [38]. Moreover, the effect of radiation, also discussed in Section 3.3, is not included for all the following results except those in Fig. 8.

3.1. The ignition process

The evolution of temperature distribution for unsuccessful and successful ignition is shown in Fig. 1. When the ignition energy is smaller than the so-called minimum ignition energy (MIE), Fig. 1a shows that the resulting flame kernel decays rapidly. This is due to the fact that the chemical heat release rate is smaller than the rate at which heat is conducted away from the kernel [16,39]. At the time around $t = 1.2$ ms, the maximum temperature is below 700 K and the chemical reaction is negligible. Therefore, it becomes an unsteady thermal conduction process in which the temperature at the center continuously decreases. For the case of successful ignition with energy deposition larger than the MIE, Fig. 1b shows that the temperature at the center initially decreases due to the termination of energy deposition and heat conduction away from the center. Subsequently, the temperature increases when the local chemical heat release rate is larger than the heat conduction rate and the flame kernel can propagate outwardly in a self-sustained manner [16,30,39].

These characteristics can be further substantiated from the flame front history, $R_f = R_f(t)$, which is defined as the position of maximum heat release rate in the simulation. Figure 2a shows the temporal variation of flame radius for stoichiometric H_2/air/He ($a = 40\%$) at different ignition energies. The MIE for this mixture, $E_{min} = 0.157$ mJ, and for all other mixtures is calculated by the method of trial-and-error with relative error below 1%. It is observed that a self-sustained propagating flame can be successfully
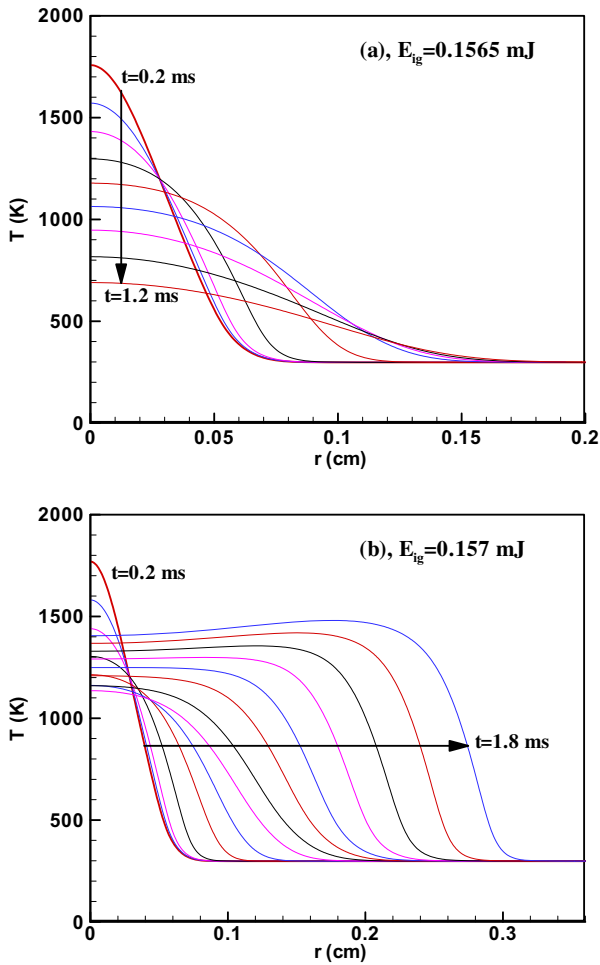
Fig. 1. Evolution of temperature distribution for (a) unsuccessful and (b) successful ignition (H$_2$/air/He, φ = 1, a = 0.4).

Fig. 2. Spherical flame initiation for H$_2$/air/He mixture (φ = 1, a = 0.4) at different ignition energies: (a), temporal variation of flame radius; (b), flame propagation speed as a function of radius.

initiated only when the ignition energy is above the MIE. The flame propagation speed, $S_b = dR_f/dt$, as a function of flame radius is presented in Fig. 2b. It is seen that the flame propagation speed changes non-monotonically with the flame radius for successful ignition: it initially decreases with the flame radius and then reverses the trend and increases after passing through a minimum speed attained at the critical flame radius. The sharp decrease of S_b is due to the termination of the ignition energy deposition at t = 0.2 ms, before which the flame kernel is over-driven by the ignition energy. The afterwards increase of S_b with R_f is due to the fact that the positive flame stretch (which reduces the flame propagation since the Markstein length of this mixture is positive, see Fig. 10 and Eq. (5)) continuously decreases during spherical flame propagation [17]. The same behavior was also observed in theoretical analyses and experiments [17,23,31,32,40–45]. Furthermore, Fig. 2b shows the Flame Speed Reverse (FSR) behavior: compared to the flame initiated by a larger ignition energy (E_{ig} = 0.158 mJ), the one initiated by a smaller energy (E_{ig} = 0.157 mJ) has larger propagation speed at R_f > 0.18 cm. The FSR was observed in experiments and transient numerical simulations for mixtures with large Markstein length [17,31]. Since the FSR cannot be predicted by quasi-steady theoretical analysis, it must originate from the unsteady flame kernel evolution [17]. The mechanism controlling the appearance of the FSR phenomenon is not well known and thus deserves further study. Figure 2b shows that the flame propagates in a quasi-steady state manner [17,42] when the flame radius is larger than 0.45 cm, and that the flame propagation speed is independent of the ignition energy for R_f > 0.45 cm.
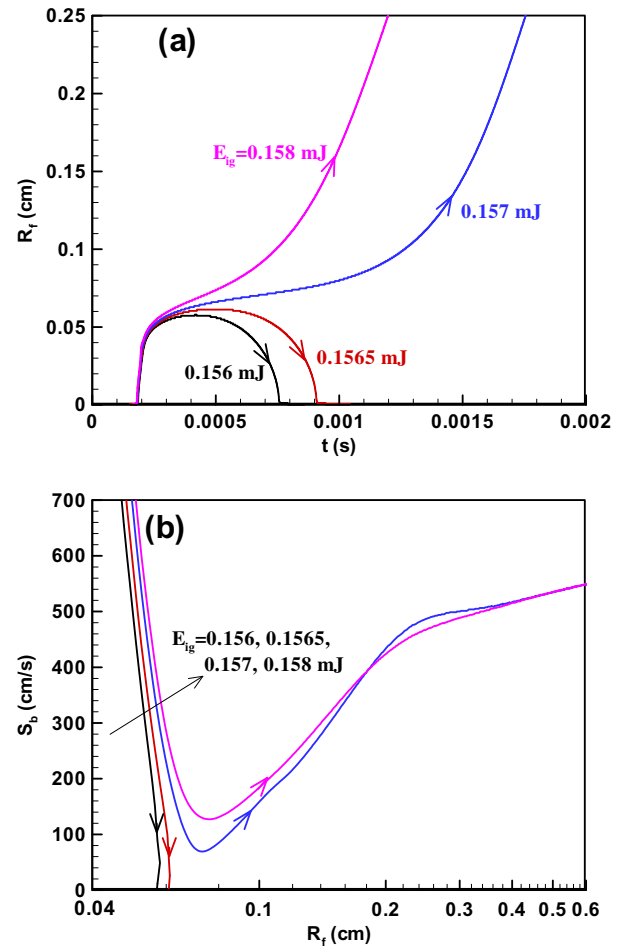
3.2. The MIE and dilution limits of stoichiometric H$_2$/air/diluent mixtures

In order to assess the effects of different diluents on the ignition of H$_2$/air mixture, simulations are conducted for stoichiometric H$_2$/air/diluent mixtures at different dilution ratios. The results are presented in Fig. 3. It is seen that for each diluent, the change of the minimum ignition energy, E_{min}, with the dilution ratio, a, consists of two regimes: in the first regime with a small value of dilution ratio, E_{min} is shown to be insensitive to a and the diluent addition has little effect on the MIE; however, in the second regime with dilution ratio above a certain value, E_{min} is shown to increase exponentially with a and the diluent addition eventually results in an infinite value of the ignition energy. It is noted that, according to our calculation for other ignition kernel sizes and times (τ_{ig} = 150 or 250 μs, r_{ig} = 150 or 250 μm), the same transition of the MIE evolution with the dilution ratio is observed as that shown in Fig. 3 (which is for τ_{ig} = 200 μs, r_{ig} = 200 μm). Figure 3 shows that, at a given dilution ratio, the diluents increase in the effectiveness based on prohibition of ignition (increasing the MIE) in the order of Ar, N$_2$, and CO$_2$, and that the MIE of He-diluted mixture is higher/lower than that of CO$_2$-diluted mixture when the dilution ratio is below/above 0.4. The different influences of dilution on the MIE are due to the different physical and chemical properties of these diluents, which will be discussed in Sections 3.3 and 3.4.

As shown in Fig. 3, for each diluent there is a critical dilution ratio or dilution limit, a_C, above which the MIE becomes infinite and
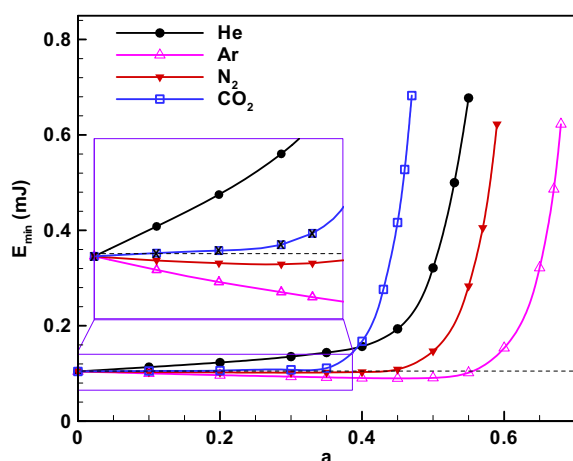
Fig. 3. Change of the MIE with the dilution ratio for stoichiometric H_2/air/diluent mixtures.

thus the mixture cannot be ignited. The value of the dilution limit for each diluent basically represents its fire-suppressant effectiveness [1–4], and it is determined via non-linear regression based on the following relationship between E_{min} and a

$$E_{min} = A \ln(a_c - a) + B \tag{3}$$

which shows that E_{min} increases exponentially with a (see Fig. 3) and $E_{min} \to \infty$ as $a \to a_c$. In Eq. (3), A and B are constants also determined by the non-linear regression, in which only data sets (a, E_{min}) in the second regime are utilized.

The dilution limits for stoichiometric H_2/air are shown in Fig. 4. Simulations for other different ignition kernel sizes and times (τ_{ig} = 150 or 250 μs, r_{ig} = 150 or 250 μm) are also conducted for CO_2 dilution and the dilution limit is found to be nearly the same (the difference is within 2%) as those shown in Fig. 4 (which is for τ_{ig} = 200 μs, r_{ig} = 200 μm). Therefore, the dilution limit is not affected by the duration and size of the ignition kernel. The experimental results reported by Qiao et al. [3] are also presented in Fig. 4. In the spherical flame experiments at micro-gravity conditions [3], the flame was ignited by a spark with gap distance adjustable in the range of 0.5–3.0 mm and the spark energy was supplied by a high-voltage capacity system with an adjustable 0–30 kV voltage and a discharge time of roughly 5 μs. Unlike the definition used in the present ignition simulation, the dilution limit is defined in experiments as the dilution ratio at which the un-

stretched laminar flame speed is reduced to $S_L \approx 2$ cm/s [3]. Therefore, the dilution limits predicted by present simulation and those measured in experiments [3] are based on completely different parameters: one on the MIE and the other on the laminar flame speed. Figure 4 shows that the dilution limits predicted by the present simulation are slightly lower than those measured in experiments (the maximum difference between them is around 5%). Nevertheless, good agreement is still achieved.
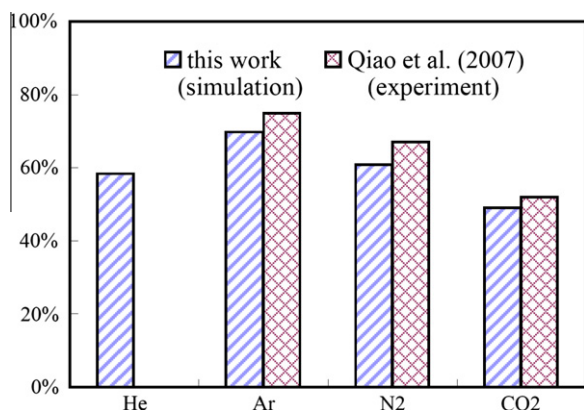
In the experiments of Qiao et al. [3], the laminar flame speed at the maximum helium dilution is above 30 cm/s, which is much larger than the near-limit flame speed ($\sim$2 cm/s) used to determine the dilution limit. Therefore, the dilution limit for helium cannot be determined based on requirement that the unstretched laminar flame speed is reduced to $S_L \approx 2$ cm/s [3,46]. The possible reason why Qiao et al. [3] cannot measure the flame speed at a higher helium dilution is that it requires extremely high ignition energy above the maximum energy that the ignition system can supply. This was mentioned in the recent paper of Qiao et al. [46] in which experiments on CH_4/air/He mixtures were conducted.

The dilution limit for each diluent is of interest because it is a measure of the efficiency of the diluents in preventing or suppressing a fire [3,46]. If the effectiveness of the diluents is evaluated based on their dilution limits in terms of ignition inhibition, the ranking is Ar < N_2 < He < CO_2 (see Fig. 4 and Table 1). This ranking is the same as the one based on the laminar flame speed [3,46]. Therefore, from the point of view of fire prevention and suppression, CO_2 is the most effective with the smallest dilution limit.

3.3. Kinetic and radiation effects of diluents

As mentioned before, many kinetic mechanisms for hydrogen oxidation are available in the literature [33–38]. Figure 5 shows the MIE predicted by different kinetic mechanisms. The dependence of the MIE on the kinetic mechanisms is shown to be noticeable only when the dilution ratio is close to the dilution limit. Moreover, the trend at which the MIE changes with the dilution ratio and the dilution limit are nearly independent of the kinetic mechanism. Therefore, only the kinetic mechanism of Li et al. [38] is used in the simulation and it is expected that the same conclusions will be drawn on the effects of dilution on hydrogen/air ignition when other mechanisms are employed.

In order to assess the kinetic effects of elementary reactions on the ignition, a sensitivity analysis of the MIE with respect to the reaction rate coefficients is conducted. In the numerical simulation, the sensitivity of the MIE to the jth elementary reaction, S_j, is defined as

$$S_j = E_{min}^j/E_{min} - 1 \tag{4}$$

where E_{min} is the MIE when all the reaction rates are kept unchanged and E_{min}^j is the MIE when only the rate of the jth elementary reaction is artificially doubled. According to the results for H_2/air/CO_2 in Fig. 6, at a low dilution ratio (a = 0% or 30%), the sensitivity is small and nearly independent of the dilution ratio. This is similar to the dependence of the MIE on the dilution ratio in the first regime (see Fig. 3 or Fig. 5). However, at a high dilution ratio (a = 40% or 45%), the sensitivity increases significantly with the dilution ratio. Therefore, the kinetic effect of diluents is important only in

Fig. 4. Dilution limits, a_c, of stoichiometric H_2/air/diluent mixtures. It is noted that the dilution limits predicted by simulation are base on the MIE while those measured in experiments are based on the laminar flame speed.

Table 1
Dilution limits, a_c, of different H_2/air/diluent mixtures.

	Ar (%)	N_2	He	CO_2
φ = 0.5	73.8	66.5	54.4	55.8
φ = 1.0	69.8	60.8	58.3	49.0
φ = 2.0	55.1	47.2	45.7	32.4
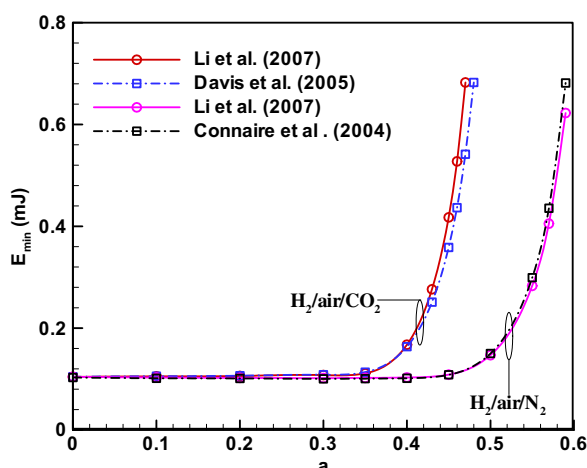
Fig. 5. The MIE of stoichiometric $H_2/air/CO_2$ and $H_2/air/N_2$ mixtures predicted by different kinetic mechanisms.
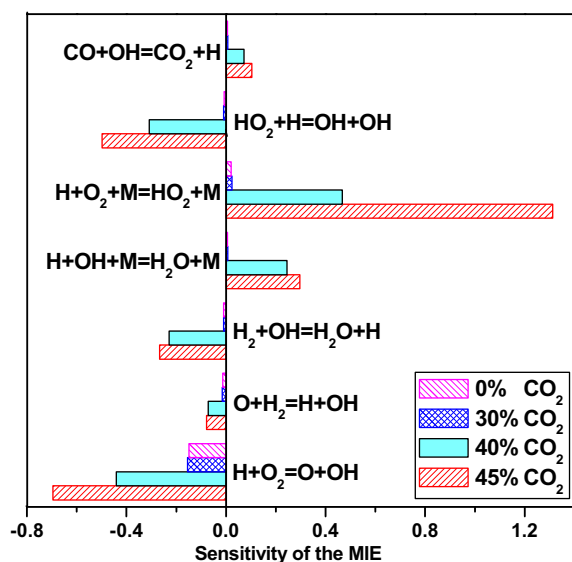
Fig. 6. Sensitivity of the MIE for stoichiometric H_2/air with different amounts of CO_2 dilution.

the second regime with dilution ratio close to the dilution limit. This explains why the dependence of the MIE on the kinetic mechanisms is noticeable only when the dilution ratio is close to the dilution limit (see Fig. 5). Similar results were reported by Qiao et al. [3] who performed sensitivity analysis of the laminar flame speed rather than the MIE. Figure 6 indicates that the three-body recombination reaction, $H + O_2 + M = HO_2 + M$, is extremely important for highly diluted near-limit mixtures. As noticed by Qiao et al. [3], this is due to the competition between chain-branching and chain-terminating reactions near the dilution limits.

It is noted that unlike He, N_2, and Ar, which are chemically inert in the ignition processes, CO_2 is chemically active and reacts with radicals (for example, $CO_2 + H = CO + OH$) [12,46]. In order to understand the kinetic effect of CO_2 dilution on the ignition process, we conduct numerical analysis using the approach similar to the work of Liu et al. [12]. An artificial species, named as inert CO_2, is introduced. The inert CO_2 has the same thermal and transport properties as the real CO_2 but it does not participate in any chemical reaction (i.e. chemically inert). Since the three-body recombination reactions are very important for highly diluted mix-

tures (see Fig. 6), we consider two types of artificial inert CO_2 in the simulation: one still acts as a three-body (the three-body coefficient of CO_2 is remained to be 3.8) and the other does not (the three-body coefficient of CO_2 is changed to be zero). The results for H_2/air diluted by three types of CO_2 are shown in Fig. 7. Consistent with the sensitivity results shown in Fig. 6, the kinetic effect of CO_2 dilution is shown to be important only at high dilution ratio. Figure 7 indicates that, for highly CO_2-diluted mixtures, the MIE can be greatly reduced if CO_2 does not react with other species but still acts as a three-body, and that the MIE can be further reduced if CO_2 does not act as a three-body. The large difference between results for the two types of artificial inert CO_2 further demonstrates the importance of the three-body recombination reactions in highly diluted near-limit mixtures. The dilution limits, a_c, for these three cases are 49.0%, 51.0%, and 54.7%, respectively. Therefore, in terms of the kinetic effect of CO_2 dilution, the dilution limit is mainly reduced by CO_2 involved in the three-body recombination reactions.

As shown in our recent study [21] and in the work of Qiao et al. [46], the radiation effect is important for spherical flame propagation of near limit mixtures. In the following, the effect of radiation on the MIE and on the dilution limit is assessed. The optically thin model [47] is used in the simulation, in which the radiation emission from CO_2, H_2O, and CO, is considered. According to the results in Fig. 8, for $H_2/air/N_2$ mixtures, the effect of radiation on the MIE and on the dilution limit is negligible. The reason for this fact is that H_2O is the only radiative species in the burned mixture and its molar fraction decreases with the dilution ratio of N_2. The same results are also obtained for $H_2/air/He$ and $H_2/air/Ar$ mixtures. However, for $H_2/air/CO_2$ mixtures, CO_2 is highly radiative and the effect of radiation on the MIE is shown to strongly depend on the dilution ratio. At a low CO_2 dilution ratio, the radiation intensity is low and thus the radiation effect on the MIE is also negligible (the relative difference between the MIE predicted by the adiabatic model and that by the radiative model is within 3% for $a \leqslant 0.4$). When the CO_2 dilution ratio is close to the dilution limit, Fig. 8 shows that the radiation effect on the MIE is noticeable: the MIE is increased by 7.5%, 11.2%, and 16.9% for $a = 0.45$, 0.46, and 0.47, respectively. However, unlike the MIE, the dilution limit of $H_2/air/CO_2$ is almost not affected by radiation (the dilution limits are 49.0% and 48.4% for the adiabatic and radiative cases, respectively). Moreover, Fig. 8 shows that the change of the MIE with the dilution ratio is not affected by radiation. Therefore, the radiation effect is not considered in all other calculations and it is expected that
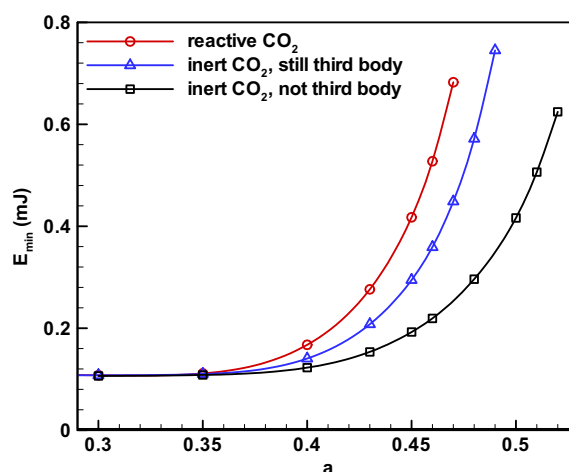
Fig. 7. Chemical effect of CO_2 on the MIE of stoichiometric $H_2/air/CO_2$ mixtures.
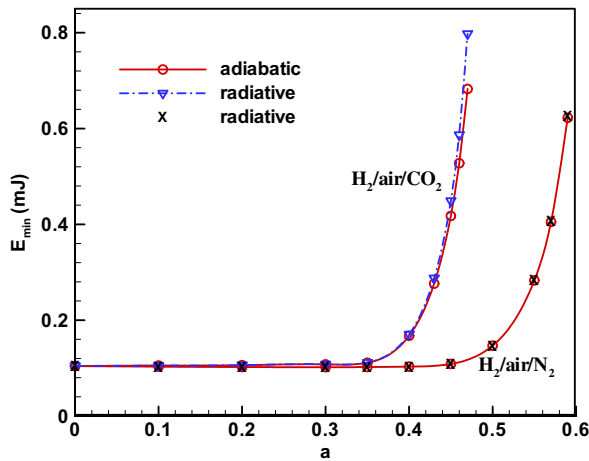
Fig. 8. Radiation effect on the MIE of stoichiometric $H_2/air/CO_2$ and $H_2/air/N_2$ mixtures.

the same conclusions will be drawn on the effects of dilution on hydrogen/air ignition even when the radiation effect is included.

3.4. Thermal and flame-dynamic effects of diluents

In order to understand the change of the MIE with the dilution ratio for different diluents (Fig. 3), the following two effects caused by dilution are analyzed: the first one is the thermal effect that dilution can reduce the adiabatic flame temperature and thus decrease the reactivity of the diluted mixture; and the second one is the flame-dynamic effect that dilution can change the Markstein length and thus affect the influence of stretch rate on the flame propagation speed of the diluted mixture. The thermal effect is characterized by the adiabatic flame temperature, T_{ad}, which is proportional to the ratio between fuel molar fraction and molar heat capacity of the mixture. Figure 9 shows that, for each diluent, the adiabatic flame temperature decreases monotonically with the dilution ratio (i.e. $dT_{ad}/da < 0$). At the same dilution ratio, we have $T_{ad, He} = T_{ad, Ar} > T_{ad, N2} > T_{ad, CO2}$ since the molar heat capacities of helium and argon are the same, both of which are lower than that of nitrogen and much lower than that of carbon dioxide. Therefore, the ranking based on the thermal effect in increasing the MIE is He = Ar < N_2 < CO_2. If only the thermal effect is considered, the MIE should always increases with the dilution ratio (this will be demonstrated by Fig. 13). However, the enlarged inset in Fig. 3
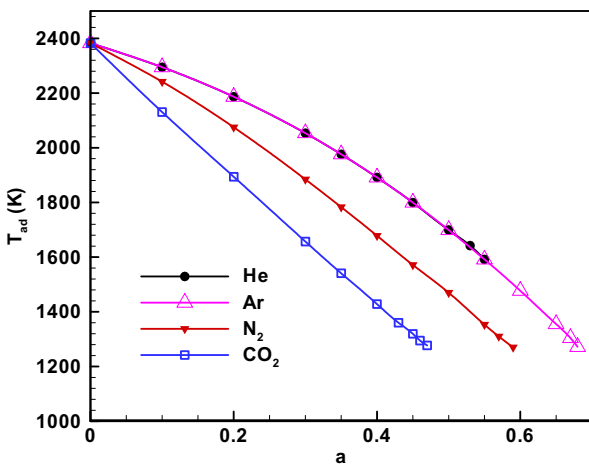
shows that E_{min} decreases with a for Ar and N_2 when the dilution ratio is below 35%. This is in fact caused by the flame-dynamic effect explained below.

It is well known that the Markstein length characterizes the variation in the local flame speed due to the influence of external stretching [48]. At moderate stretch rate, the stretched flame propagation speed, S_b, can be considered to vary linearly with the stretch rate, K [48]

$$S_b = S_b^0 - L_b K \qquad (5)$$

where S_b^0 and L_b are, respectively, the unstretched laminar flame speed and Markstein length with respect to the burned mixture. For a propagating spherical flame, the stretch rate, $K = 2S_b/R_f$, is inversely proportional to the flame radius [48]. Therefore, for an ignition kernel with small radius (around 0.5 mm, see Fig. 1), its propagation speed is strongly affected by the large positive stretch rate according to Eq. (5) if the Markstein length is not close to zero [23,40]. Depending on the value of the Markstein length, L_b, the flame kernel propagation can be either promoted (for $L_b < 0$) or inhibited (for $L_b > 0$) by the positive stretch rate. As a result, the MIE depends strongly on the Markstein length: the larger the Markstein length, the larger the MIE. The validity of this conclusion was demonstrated by theoretical analysis and numerical simulation conducted in Ref. [23] and will also be confirmed by results in Fig. 12. Therefore, the Markstein length can be used to characterize the flame-dynamic effect of dilution on ignition.

The Markstein length, L_b, is obtained from the linear extrapolation between S_b and K according to Eq. (5). Figure 10 shows the change of Markstein length with the dilution ratio for different diluents. It is seen that, for helium dilution, L_b increases monotonically with a (i.e. $dL_b/da > 0$); while for other diluents (Ar, N_2, and CO_2), L_b decreases monotonically with a (i.e. $dL_b/da < 0$). Moreover, the magnitude of the gradient, $|dL_b/da|$, is shown to increase with the dilution ratio, indicating that the flame-dynamic effect becomes stronger at higher dilution ratio. The change of L_b with a can be explained with the help of the following relationship [48]

$$\frac{L_b}{\delta} = \frac{\ln(1/\sigma)}{1 - \sigma} + \frac{A(Le - 1)}{2} \left[\sigma \int_0^{(1/\sigma)-1} \frac{\ln(1 + x)}{x} dx \right] \qquad (6)$$

where δ, σ, A, and Le are, respectively, the adiabatic planar flame thickness, the density ratio between burned and unburned gases, the activation temperature normalized by the temperature of unburned gas, and the Lewis number. With the increase of the dilution ratio, δ, σ, and A all increase. It can be easily shown that the term inside the square brackets in Eq. (6) increases quickly with the

Fig. 9. Change of the adiabatic flame temperature with the dilution ratio for stoichiometric $H_2/air/diluent$ mixtures.
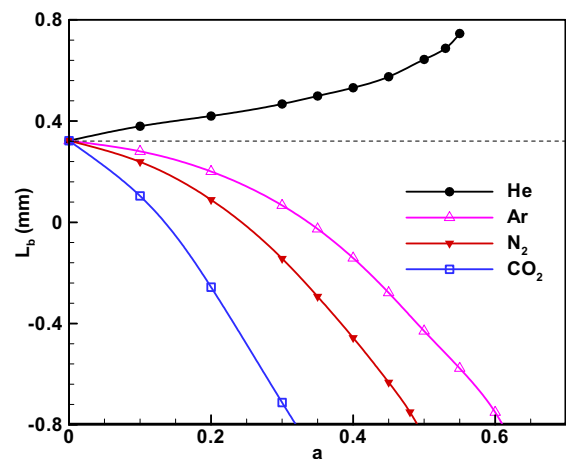
Fig. 10. Change of the Markstein length with the dilution ratio for stoichiometric $H_2/air/diluent$ mixtures.

density ratio and so does it with the dilution ratio. Moreover, the thermal diffusivity, $\lambda/(\rho C_P)$, and thus the Lewis number, $Le = \lambda/(\rho C_P D)$, increases (decreases) with the dilution ratio for He (Ar, N_2, CO_2). According to Eq. (6), L_b should increase (decrease) with the dilution ratio for He (Ar, N_2, CO_2). Therefore, the numerical results shown in Fig. 10 are consistent with Eq. (6) derived from asymptotic analysis [48].

The change of the MIE with the dilution ratio for different diluents (see Fig. 3) is mainly caused by the thermal and flame-dynamic effects introduced above:

$$\frac{dE_{\min}}{da} \approx G_T \times \frac{dT_{ad}}{da} + G_L \times \frac{dL_b}{da} \qquad (7)$$

where $G_T = \partial E_{min}/\partial T_{ad}$ and $G_L = \partial E_{min}/\partial L_b$, respectively, represent the influence/intensity of the thermal effect and flame-dynamic effect on the MIE. It is noted that Eq. (7) is an approximation since the MIE depends on other factors besides T_{ad} and L_b. Moreover, the Markstein length depends on several parameters such as thermal diffusivity, mass diffusivity, activation energy and density ratio (see Eq. (6)). Since these parameters change together with the dilution ratio, it is difficult to evaluate more precisely the relative impact of each parameter. The influences of dilution on the adiabatic flame temperature (dT_{ad}/da) and Markstein length (dL_b/da) have been obtained (see Figs. 9 and 10). In order to explain the change of the MIE with dilution, we need know how G_T and G_L are affected by the dilution ratio.

To demonstrate the flame-dynamic effect on ignition, the thermal effect should be fixed: only the Markstein length changes while the adiabatic flame temperature is kept constant. Using the same approach employed in our previous study [23], the H_2/air/He/Ar mixtures are considered in numerical simulations. Figure 11 shows the results for mixtures in which the volumetric fractions of helium and argon are changed while their sum is fixed to be 55%. With the increase of the helium fraction, a_{He} (thus the decrease of the argon fraction, $a_{Ar} = 0.55 - a_{He}$), the Markstein length is shown to increase since the thermal conductivity of the mixture increases. However, as shown in Fig. 11, the adiabatic flame temperature remains unchanged with the helium fraction since the molar heat capacities of helium and argon are the same. Therefore, the influ-

ence of the thermal effect on ignition is fixed while that of the flame-dynamic effect changes with the helium fraction. In order to reveal the influence of the flame-dynamic effect on the MIE, Fig. 12 shows the change of the MIE with L_b. As expected, the MIE is shown to monotonically increase with the Markstein length (i.e. $G_L = \partial E_{min}/\partial L_b > 0$) when the adiabatic flame temperature is kept constant. More importantly, Fig. 12 indicates that G_L decreases with T_{ad} and increases with L_b. For He dilution, T_{ad} decreases with a (see Fig. 9) and L_b increases with a (see Fig. 10). Consequently, G_L increases quickly with a for H_2/air/He (see the dashed line AC on Fig. 12). While for other diluents (Ar, N_2, and CO_2), both T_{ad} and L_b decreases with a. Therefore, the dependence of G_L on a becomes weaker compared to that of He dilution. It is found that for Ar dilution (see the dashed line AB in Fig. 12), G_L increases moderately with a.

Similarly, to demonstrate the thermal effect on ignition, the flame-dynamic effect should be fixed: only the adiabatic flame temperature changes while the Markstein length is kept constant. Figure 13 shows the change of the MIE with T_{ad}. The MIE is shown to monotonically decrease with the adiabatic flame temperature (i.e. $G_T = \partial E_{min}/\partial T_{ad} < 0$) when the Markstein length is kept constant. Moreover, Fig. 13 shows that the magnitude of the gradient, $|G_T|$, increases (decreases) exponentially with the dilution ratio (the adiabatic flame temperature). Therefore, the thermal effect increases significantly when the dilution limit is approached.

Since only a very limited number of cases (represented by the symbols in Figs. 9–12) are studied in simulation, the accurate values of these gradients, dT_{ad}/da, dL_b/da, G_L, and G_T, are not obtained. Nevertheless, together with Eq. (7), the qualitative information on dT_{ad}/da, dL_b/da, G_L, and G_T indicated by Figs. 9, 10, 12 and 13, respectively, is still helpful for understanding the change of the MIE with the dilution ratio shown in Fig. 3. For He, the thermal and flame-dynamic effects both prohibit ignition ($G_T \times dT_{ad}/da > 0$ and $G_L \times dL_b/da > 0$) and thus the MIE monotonically increases with the dilution ratio ($dE_{min}/da > 0$). Moreover, as mentioned in the discussions related to Figs. 12 and 13, both $|G_T|$ and G_L increases significantly with a when the dilution limit is approached. This results in the exponential increase of E_{min} with a in the second regime, which is consistent with results for H_2/air/He shown in Fig. 3.

For CO_2, the thermal effect (which prohibits ignition since $G_T \times dT_{ad}/da > 0$) should always dominate over the flame-dynamic effect (which promotes ignition since $G_L \times dL_b/da < 0$) so that the
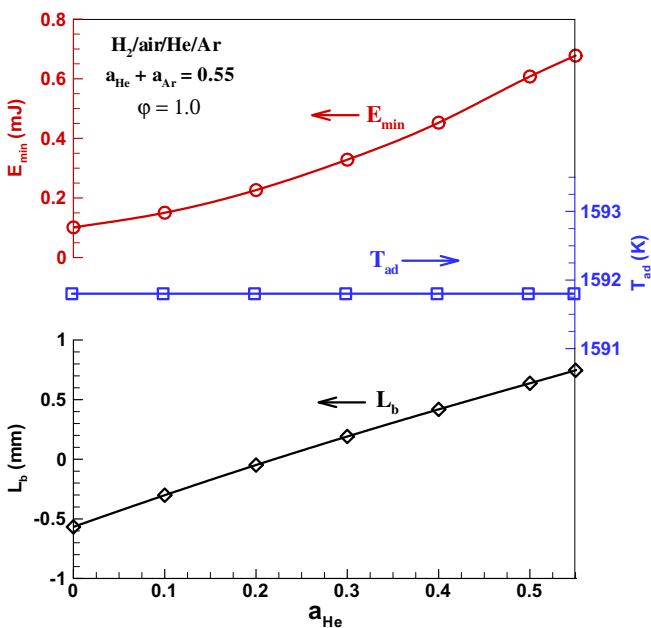
Fig. 11. The MIE, adiabatic flame temperature, and Markstein length of stoichiometric H_2/air/He/Ar mixtures.
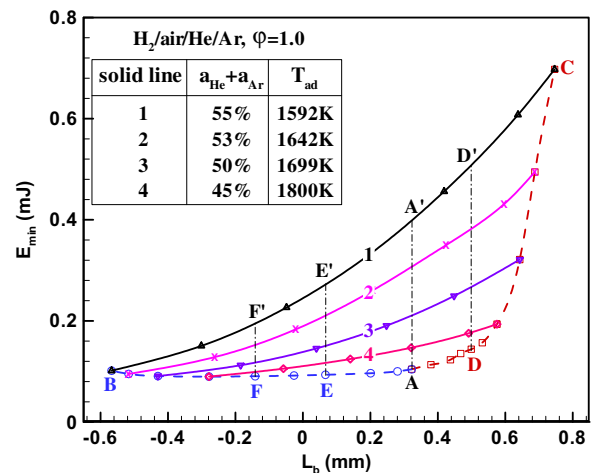
Fig. 12. Change of the MIE with the Markstein length for stoichiometric H_2/air/He/Ar mixtures. Point A represents results for stoichiometric H_2/air without He or Ar addition. The dashed lines, AEFB and ADC, represent results for stoichiometric H_2/air/Ar and H_2/air/He mixtures, respectively. Each solid line represents results for mixtures which have the same adiabatic flame temperature and each dash-dotted line for mixtures with the same Markstein length.
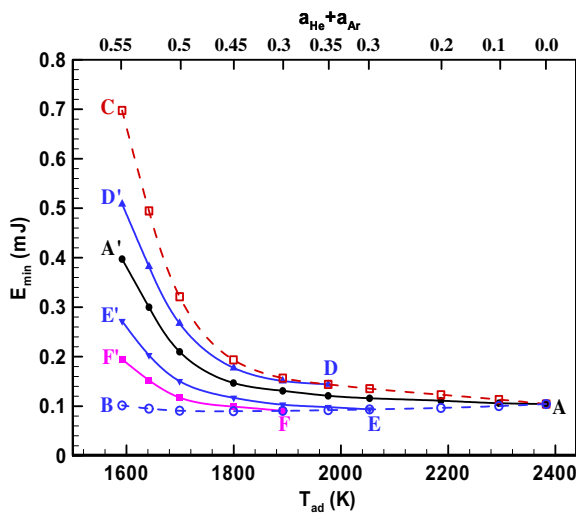
Fig. 13. Change of the MIE with the adiabatic flame temperature for stoichiometric H_2/air/He/Ar mixtures. On each solid line (AA′, DD′, EE′ and FF′), the Markstein length is constant (see the dash-dotted lines in Fig. 12). The dashed lines, AEFB and ADC, represent results for stoichiometric H_2/air/Ar and H_2/air/He mixtures, respectively (same as those in Fig. 12).

MIE monotonically increases with the dilution ratio ($dE_{min}/da > 0$, see Fig. 3). Compared to He dilution, at a small dilution ratio, the flame-dynamic effect makes $(dE_{min}/da)_{CO2}$ smaller than $(dE_{min}/da)_{He}$. Therefore, the MIE of H_2/air/CO_2 is smaller than that of H_2/air/He when the dilution ratio is below 0.4. However, as shown in Fig. 13, $|G_T|$ increases (decreases) quickly with a (T_{ad}) at high dilution ratio. Since $T_{ad, CO2}$ is much lower than $T_{ad, He}$ at the same a (see Fig. 9), it will be expected that, at high dilution ratio, $|G_T|_{CO2}$ is much larger than $|G_T|_{He}$. This results in a larger value of dE_{min}/da for H_2/air/CO_2 than that for H_2/air/He. Consequently, as shown in Fig. 3, the MIE of H_2/air/CO_2 is larger than that of H_2/air/He at high dilution ratio.

For Ar and N_2 at a small value of dilution ratio (in the first regime), the flame-dynamic effect (which promotes ignition since $G_L \times dL_b/da < 0$) dominates over the thermal effect (which prohibits ignition since $G_T \times dT_{ad}/da > 0$) so that, as shown in Fig. 3, the MIE decreases with dilution ratio (i.e. $dE_{min}/da < 0$). However, at a large value of dilution ratio ($a > 56\%$ for Ar and $a > 43\%$ for N_2), the thermal effect dominates over the flame-dynamic effect and thus the MIE increases with the dilution ratio (i.e. $dE_{min}/da > 0$). Again, this is due to the fact that $|G_T|$ increases quickly with a at high dilution ratio (see Fig. 13). Therefore, the non-monotonic change of the MIE with the dilution ratio for Ar and N_2 is caused by the competition between the thermal and flame-dynamic effects. Compared to He at the same dilution ratio, the MIE for Ar is always lower. This is because the thermal effect of Ar dilution is the same as that of He dilution, while the flame-dynamic effect promotes and prohibits ignition for Ar and He dilution, respectively. Fig. 3 shows that the transition between the first and second regimes occurs at different dilution ratios (denoted by a^*) for different diluents: $a^*_{CO2} < a^*_{He} < a^*_{N2} < a^*_{Ar}$. According to Fig. 13, G_L increases significantly with a (so does dE_{min}/da) when the adiabatic flame temperature is low enough (i.e. the dilution limit is approached). Therefore the transition dilution ratio depends on the adiabatic flame temperature. Since the adiabatic flame temperature for CO_2 dilution is the lowest while that for Ar dilution is the highest (see Fig. 9), we have $a^*_{CO2} < a^*_{N2} < a^*_{Ar}$. Unlike other diluents, for He, the thermal and flame dynamic effects both prohibit ignition. Therefore, the transition dilution ratio of He, a^*_{He}, becomes lower than those of N_2 and Ar.

3.5. Results for lean and rich H_2/air/diluent mixtures

Besides the stoichiometric case, both fuel lean ($\varphi = 0.5$) and rich ($\varphi = 2.0$) H_2/air/diluent mixtures at atmospheric pressure are studied and the results of the MIE are shown in Fig. 14. Similar to the results for the stoichiometric case (Fig. 3), two regimes are also observed in the change of the MIE with the dilution ratio for the fuel lean and rich cases. Moreover, Fig. 14 shows that for a given dilution ratio, the diluents increase in the effectiveness based on prohibition of ignition (increasing the MIE) in the order of Ar, N_2, and CO_2, which is the same as the stoichiometric case. The transition of the MIE evolution with the dilution ratio is caused by the thermal and flame-dynamic effects discussed above for the stoichiometric case.

For fuel lean and rich H_2/air/diluent mixtures, the dilution limits are also determined via non-linear regression based on Eq. (3). The results are presented in Table 1. It is seen that the results for the fuel rich cases are similar to those for stoichiometric case and the ranking in terms of the effectiveness on ignition inhibition is also Ar < N_2 < He < CO_2. Therefore, CO_2 has the smallest dilution limit and is the most effective in fire prevention and suppression for H_2/air flames at stoichiometric and fuel rich cases. However, for the fuel lean case ($\varphi = 0.5$), the dilution limit for He is slightly lower than that of CO_2. Figure 15 shows the MIE, adiabatic flame temperature, and Markstein length for different H_2/air/CO_2 mixtures. When the adiabatic flame temperature is the same ($T_{ad,A} = T_{ad,B}$), the MIE increases with the Markstein length ($L_{b,A} < L_{b,B}$, $E_{min,A} < E_{min,B}$); when the Markstein length is the same ($L_{b,A} = L_{b,C}$),
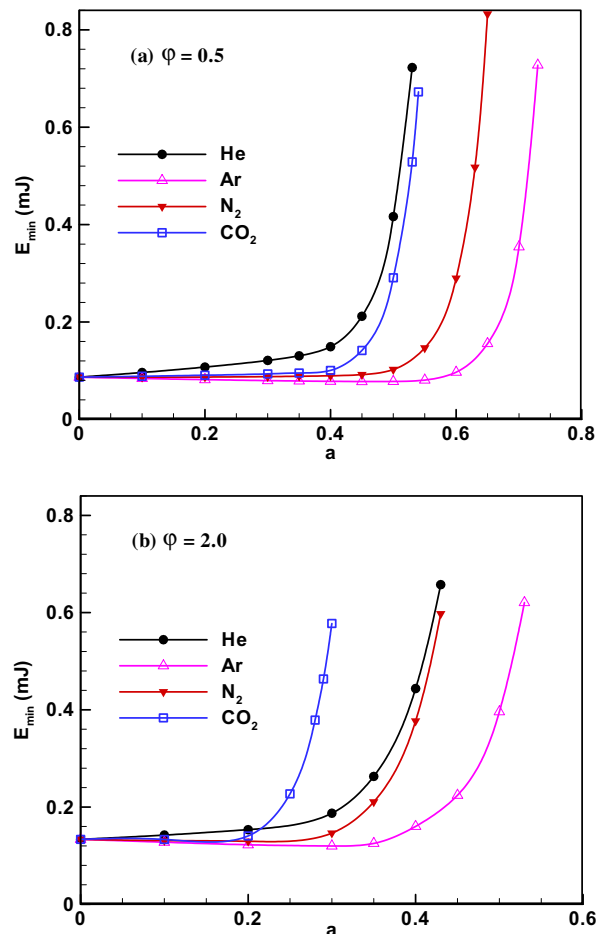
Fig. 14. Change of the MIE with the dilution ratio for (a) fuel lean and (b) fuel rich H_2/air/diluent mixtures.
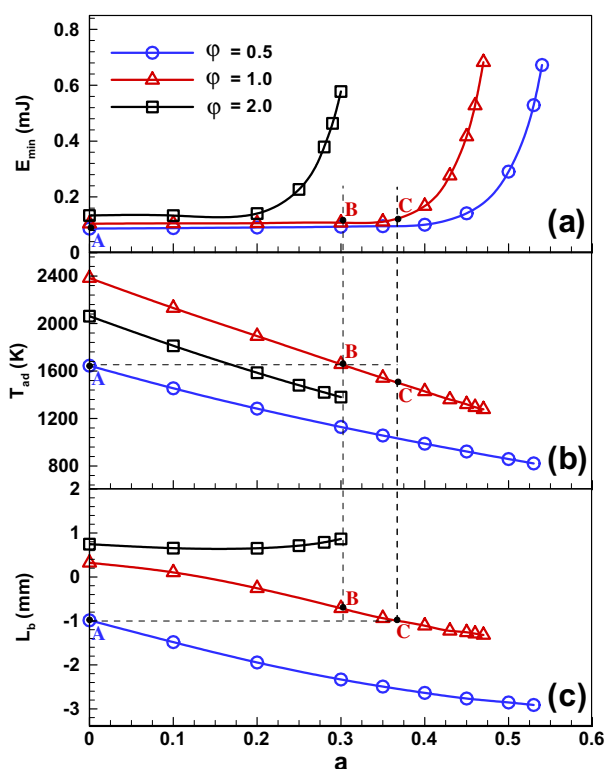
Fig. 15. Effects of equivalence ratio on the (a) MIE, (b) adiabatic flame temperature, and (c) Markstein length of H_2/air/CO_2 mixtures.

the MIE decreases with the adiabatic flame temperature ($T_{ad,A}$ > $T_{ad,C}$, $E_{min,A}$ < $E_{min,C}$). At the same dilution ratio, Fig. 15b shows that the adiabatic flame temperature of the fuel lean mixture (φ = 0.5) is about 300 K lower than that of the fuel rich case (φ = 2.0), and about 600 K lower than the stoichiometric case (φ = 1.0). However, Fig. 15a shows that the MIE of the fuel lean mixture is the lowest. This is because the Markstein length of the fuel lean mixture is negative and much smaller than those of fuel rich and stoichiometric mixtures (Fig. 15c). It is the flame-dynamic effect that makes the ignition of lean mixture much easier. Furthermore, Fig. 15a shows that for $0.5 \leqslant \varphi \leqslant 2.0$, the dilution limit decreases with the equivalence ratio. This is due to the fact that the Markstein length of H_2/air decreases with the equivalence ratio and thus the flame-dynamic effect makes ignition more difficult at a higher equivalence ratio.

4. Conclusions

Numerical simulations of the ignition process are conducted for different H_2/air/diluent (He, Ar, N_2, and CO_2) mixtures. The minimum ignition energies for different diluents at different dilution ratios are obtained. The dilution limits for fuel lean, stoichiometric, and fuel rich H_2/air/diluent mixtures are reported. The main conclusions are:

1. For each diluent, the change of the MIE with the dilution ratio consists of two regimes: in the first regime the diluent addition has little effect on the MIE; and in the second regime the MIE increases exponentially with the dilution ratio and the diluent addition will eventually results in an infinite value of the ignition energy. Results for stoichiometric H_2/air/diluent mixtures show that, at a given dilution ratio, the diluents increase in the effectiveness based on the prohibition of ignition (increasing the MIE) in the

order of Ar, N_2, and CO_2, and that the MIE of He-diluted mixture is higher/lower than that of CO_2-diluted mixture when the dilution ratio is below/above 0.4.

2. The dilution limits for stoichiometric H_2/air mixtures are obtained and compared with those measured in micro-gravity experiments by Qiao et al. [3]. Good agreement is achieved between the dilution limits based on the MIE (present simulation) and those on the laminar flame speed (experiments by Qiao et al. [3]). The ranking in terms of the effectiveness in ignition inhibition is shown to be Ar < N_2 < He < CO_2. Therefore, CO_2 has the smallest dilution limit and is the most effective on fire prevention and suppression for H_2/air flames.

3. The kinetic effect of dilution is assessed by conducting sensitivity analysis and artificially setting CO_2 to be inert. It is found that the kinetic effect is important only in the second regime with dilution ratio close to the dilution limit. Therefore, the dependence of the MIE on the kinetic mechanisms is noticeable only for large dilution ratio. The three-body recombination reaction, $H + O_2 + M = HO_2 + M$, is shown to be extremely important for highly diluted near-limit mixtures. Therefore, in terms of the kinetic effect of CO_2 dilution, the dilution limit is mainly reduced by CO_2 involved in the three-body recombination reactions.

4. The effect of radiation on the MIE and on the dilution limit is assessed. For N_2, He and Ar, the effect of radiation on the MIE and on the dilution limit is negligible. For H_2/air/CO_2 mixtures, only when the dilution ratio is close to the dilution limit will the radiation effect on the MIE be noticeable, while the dilution limit and the transition of the MIE evolution with the dilution ratio are almost not affected by radiation.

5. The thermal and flame-dynamic effects of dilution, characterized by the adiabatic flame temperature and Markstein length, respectively, are discussed. The thermal effect always prohibits ignition and the ranking based on the thermal effect in increasing the MIE is He = Ar < N_2 < CO_2. However, when only the flame-dynamic effect is considered, the ignition process is prohibited (promoted) by He (Ar, N_2, CO_2) dilution since the Markstein length of the diluted mixture increases (decreases) with the dilution ratio. The influence of the thermal effect ($G_T = \partial E_{min}/\partial T_{ad}$) and flame-dynamic effect ($G_L = \partial E_{min}/\partial L_b$) on the MIE is assessed using H_2/air/He/Ar mixtures. For He, the thermal and flame-dynamic effects both prohibit ignition and thus the MIE monotonically increases with the dilution ratio; while for Ar, N_2, and CO_2, the change of the MIE with the dilution ratio is caused by the competition between the thermal effect (which prohibits ignition) and flame-dynamic effect (which promotes ignition). Since the influence of thermal effect becomes significant when the dilution limit is approached, the MIE increases exponentially with the dilution ratio in the second regime for all these diluents.

References

[1] J.L. Bryan, Fire Suppression and Detection Systems, Macmillan Publishing Company, New York, 1989.
[2] L. Qiao, C.H. Kim, G.M. Faeth, Combust. Flame 143 (2005) 79–96.
[3] L. Qiao, Y.X. Gu, W.J.A. Dam, E.S. Oran, G.M. Faeth, Proc. Combust. Inst. 31 (2007) 2701–2709.

[4] L. Qiao, Y. Gu, W.J.A. Dam, E.S. Oran, G.M. Faeth, Combust. Flame 151 (2007) 196–208.
[5] H. Tsuji, I. Yamaoka, Proc. Combust. Inst. 13 (1971) 723–731.
[6] N. Saito, Y. Ogawa, Y. Saso, C.H. Liao, R. Sakei, Fire Saf. J. 27 (1996) 185–200.
[7] C. Liao, N. Saito, Y. Saso, Y. Ogawa, Fire Saf. J. 27 (1996) 49–68.
[8] J. Park, J.S. Kim, J.O. Chung, J.H. Yun, S.I. Keel, Int. J. Hydrogen Energy 34 (2009) 8756–8762.
[9] J. Park, D.H. Lee, S.H. Yoon, T.M. Vu, J.H. Yun, S.I. Keel, Int. J. Hydrogen Energy 34 (2009) 1578–1584.
[10] S.T. Tang, M.K. Chernovsky, H.G. Im, A. Atreya, Combust. Flame 157 (2010) 118–126.
[11] S.T. Tang, H.G. Im, A. Atreya, Combust. Flame 157 (2010) 127–136.
[12] F.S. Liu, H.S. Guo, G.J. Smallwood, Combust. Flame 133 (2003) 495–497.
[13] Z. Chen, X. Qin, B. Xu, Y.G. Ju, F.S. Liu, Proc. Combust. Inst. 31 (2007) 2693–2700.
[14] F. Halter, F. Foucher, L. Landry, C. Mounaim-Rousselle, Combust. Sci. Technol. 181 (2009) 813–827.
[15] E.J. Hu, Z.H. Huang, J.J. He, C. Jin, H.Y. Miao, X.B. Wang, Chin. Sci. Bull. 54 (2009) 846–857.
[16] B. Lewis, G. Von Elbe, Combustion Flames and Explosive of Gases, Academic Press, New York, 1961.
[17] Z. Chen, M.P. Burke, Y. Ju, Proc. Combust. Inst. 32 (2009) 1253–1260.
[18] Z. Chen, M.P. Burke, Y. Ju, Combust. Theor. Model. 13 (2009) 343–364.
[19] Z. Chen, Int. J. Hydrogen Energy 34 (2009) 6558–6567.
[20] W. Sun, Z. Chen, X. Gou, Y. Ju, Combust. Flame 157 (2010) 1298–1307.
[21] Z. Chen, Combust. Flame 157 (2010) 2267–2276.
[22] Z. Chen, Combust. Flame 158 (2011) 291–300.
[23] Z. Chen, M.P. Burke, Y. Ju, Proc. Combust. Inst. 33 (2011) 1219–1226.
[24] G. Strang, SIAM J. Numer. Anal. 5 (1968) 506–517.
[25] P.N. Brown, G.D. Byrne, A.C. Hindmarsh, SIAM J. Sci. Stat. Comput. 10 (1989) 1038–1051.
[26] R.J. Kee, J.F. Grcar, M.D. Smooke, J.A. Miller, Sandia National Laboratory Report SAND85-8240, 1985.
[27] R.J. Kee, F.M. Rupley, J.A. Miller, Sandia National Laboratory Report SAND89-8009B, 1989.
[28] M. Sun, K. Takayama, J. Comput. Phys. 150 (1999) 143–180.
[29] A. Frendi, M. Sibulkin, Combust. Sci. Technol. 73 (1990) 395–413.
[30] H.J. Kim, S.H. Chung, C.H. Sohn, KSME Int. J. 18 (2004) 838–846.
[31] A.P. Kelley, G. Jomaas, C.K. Law, Combust. Flame 156 (2009) 1006–1013.
[32] C.L. Tang, J.J. He, Z.H. Huang, C. Jin, J.H. Wang, X.B. Wang, H.Y. Miao, Int. J. Hydrogen Energy 33 (2008) 7274–7285.
[33] J. Li, Z.W. Zhao, A. Kazakov, F.L. Dryer, Int. J. Chem. Kinet. 36 (2004) 566–575.
[34] M.O. Conaire, H.J. Curran, J.M. Simmie, W.J. Pitz, C.K. Westbrook, Int. J. Chem. Kinet. 36 (2004) 603–622.
[35] A.A. Konnov, Combust. Flame 152 (2008) 507–528.
[36] S.G. Davis, A.V. Joshi, H. Wang, F. Egolfopoulos, Proc. Combust. Inst. 30 (2005) 1283–1292.
[37] P. Saxena, F.A. Williams, Combust. Flame 145 (2006) 316–323.
[38] J. Li, Z.W. Zhao, A. Kazakov, M. Chaos, F.L. Dryer, J.J. Scire, Int. J. Chem. Kinet. 39 (2007) 109–136.
[39] P.D. Ronney, Opt. Eng. 33 (1994) 510–521.
[40] Z. Chen, Y. Ju, Combust. Theor. Model. 11 (2007) 427–453.
[41] M. Champion, B. Deshaies, G. Joulin, K. Kinoshita, Combust. Flame 65 (1986) 319–337.
[42] D. Bradley, P.H. Gaskell, X.J. Gu, Combust. Flame 104 (1996) 176–198.
[43] X.L. Gu, Z.H. Huang, S. Wu, Q.Q. Li, Combust. Flame 157 (2010) 2318–2325.
[44] Y. Ko, R.W. Anderson, V.S. Arpaci, Combust. Flame 83 (1991) 75–87.
[45] H. Zhang, Z. Chen, Combust. Flame 158 (2011), doi:10.1016/j.combustflame.2010.12.031.
[46] L. Qiao, Y. Gan, T. Nishiie, W.J.A. Dam, E.S. Oran, Combust. Flame 157 (2010) 1446–1455.
[47] Y. Ju, H.S. Guo, F.S. Liu, K. Maruta, J. Fluid Mech. 379 (1999) 165–190.
[48] P. Clavin, Prog. Energy Combust. Sci. 11 (1985) 1–59.